Article ID: 1003－6326(2004)04－0686－06

Hot-press sintering of MA Fe-based nanocrystalline/amorphous soft magnetic powder①

LU Bin(卢 斌)[1], YI Dan-qing(易丹青)[1], YAN Biao(严 彪)[2], YIN Jun-lin(殷俊林)[2], LIU Hui-qun(刘会群)[1], WU Biao-li(吴标理)[1], CHEN Xiao-li(陈小丽)[1]

(1. School of Materials Science and Engineering, Central South University, Changsha 410083, China; 2. Institute of Materials Science and Engineering, Tongji University, Shanghai 200092, China)

Abstract: Microstructures and magnetic properties of $Fe_{84}Nb_7B_9$, $Fe_{80}Ti_8B_{12}$ and $Fe_{32}Ni_{36}(Nb/V)_7Si_8B_{17}$ powders and their bulk alloys prepared by mechanical alloying(MA) method and hot-press sintering were studied. The results show that: 1) After MA for 20 h, nanocrystalline bcc single phase supersaturated solid solution forms in $Fe_{84}Nb_7B_9$ and $Fe_{80}Ti_8B_{12}$ alloys, amorphous structure forms in $Fe_{32}Ni_{36}Nb_7Si_8B_{17}$ alloy, duplex microstructure composed of nanocrystalline γ-(FeNi) supersaturated solid solution and trace content of Fe_2B phase forms in $Fe_{32}Ni_{36}V_7Si_8B_{17}$ alloy. 2) The decomposition process of supersaturated solid solution phases in $Fe_{84}Nb_7B_9$ and $Fe_{80}Ti_8B_{12}$ alloys happens at 710－780 ℃, crystallization reaction in $Fe_{32}Ni_{36}Nb_7Si_8B_{17}$ alloy happens at 530 ℃(the temperature of peak value) and residual amorphous crystallized further happens at 760 ℃ (the temperature of peak value), phase decomposition process of supersaturated solid solution at 780 ℃ (the temperature of peak value) and crystallization reaction at 431 ℃ (the temperature of peak value) happens in $Fe_{32}Ni_{36}V_7Si_8B_{17}$ alloy. 3) under 900 ℃, 30 MPa, 0.5 h hot-press sintering conditions, bulk alloys with high relative density(94.7%－95.8%) can be obtained. Except that the grain size of $Fe_{84}Nb_7B_9$ bulk alloy is large, superfine grains (grain size 50－200 nm) are obtained in other alloys. Except that single phase microstructure is obtained in $Fe_{80}Ti_8B_{12}$ bulk alloy, multi-phase microstructures are obtained in other alloys. 4) The magnetic properties of $Fe_{80}Ti_8B_{12}$ bulk alloy(B_s= 1.74 T, H_c= 4.35 kA/m) are significantly superior to those of other bulk alloys, which is related to the different phases of nanocrystalline or amorphous powder formed during hot-press sintering process and grain size.

Key words: Fe-based soft magnetic alloys; high energy milling; hot-press sintering; amorphous phase; magnetic properties

CLC number: TG 139 **Document code:** A

1 INTRODUCTION

Compared with Fe-based amorphous alloys the nanocrystalline alloys of Fe-Si-B-Nb-Cu and Fe-(Zr, Hf, Nd)-B systems[1-4] have better soft magnetic properties and higher saturation induction density. Therefore, since the $Fe_{73.5}Si_{13.5}B_9Nb_3Cu_1$ nanocrystalline was found by Yoshizawa et al[1] in 1988, many countries attached great importance to the researching of these nanocrystalline alloys. However, soft magnetic alloys were mostly used in bulks (complex shape) in engineering applications. At present, the shape and size of soft magnetic nanocrystalline alloys obtained generally by melt-spinning technique are limited, only ribbon and powder can be available. So, how to obtain nanocrystalline/amorphous bulk alloys from these amorphous soft magnetic powder or ribbon became the attention focus of researchers[5-14].

Mechanical alloying (MA) known as an efficient method of preparing metastable material were attentioned generally by researchers. Compared with melt-spinning, MA owns the advantages of simple process, high yield and easy production in large scale, and powders obtained by MA have better flowing property and compressibility. By this means nanocrystalline soft magnetic bulk alloys by hot-press sintering of MA nanocrystalline/amorphous soft magnetic powders can be prepared. It is reported in some references[15-21] that Fe-based amorphous/nanocrystalline soft magnetic powder can be prepared by the method of MA, but the reports of getting nanocrystalline soft magnetic bulk alloy by hot-press sintering are few.

With high activation energy the sintering temperature of MA nanocrystalline powder decreases. During the sintering process, for amorphous and nanocrystalline supersaturated solid solution, it's hard to avoid the grain growth coarsening of nanocrystalline microstructure, the decomposition of supersaturated solid solution and the crystallization of amorphous alloys. These transformations in sintering pro-

① **Foundation item:** Project(01YJJ2056) supported by the Natural Science Foundation of Hunan Province, China

Received date: 2004－01－06; **Accepted date:** 2004－03－19

Correspondence: LU Bin, Associate Professor, PhD; Tel: +86-731-8836319; E-mail: luoffice@mail.csu.edu.cn

cess are harmful to the soft magnetic properties of alloy, however, if nanoparticles with high thermal stability and diffusible distribution precipitate during this process, with the hindrance of these particles to crystal boundary migration, superfine grains can be obtained. Apparently, it is necessary to study these materials if we can get single phase superfine bulk alloys with high density and good soft magnetic properties prepared by the hot-press sintering under low temperatures.

Microstructure and magnetic properties of $Fe_{84}Nb_7B_9$, $Fe_{80}Ti_8B_{12}$ and $Fe_{32}Ni_{36}(Nb/V)_7Si_8B_{17}$ powders and their bulk alloys prepared by MA method and hot-press sintering were studied in this paper.

2 EXPERIMENTAL

$Fe_{84}Nb_7B_9$, $Fe_{80}Ti_8B_{12}$ and $Fe_{32}Ni_{36}(Nb/V)_7Si_8B_{17}$ prepared by Ni, Nb, Ti, V, Si and B powders with a high purity of 99.5% and size of 75 μm. FriTSCH Pulverisette-5 planetary ball milling machine was used in this experiment. Stainless steel balls and stainless steel tank were prepared for ball-milling, and protecting argon was taken to prevent the oxidation of samples. The ratio of griding media to material is 15∶1, rotational speed is 300 r/min, AFVPHP-R-10 multifunction high temperature furnace was used in hot-press sintering experiment, with argon protection, pressure p = 30 MPa, sintering temperature t = 900 ℃, holding time= 0.5 h. Dmax-rA X-ray diffraction system, Cu target and K_α spectrum was used in the X-ray diffraction experiment. The average grain size is given by the Scherrer equation $d = 0.91\lambda/(B\cos\theta)$, in which d is the average grain size, λ indicates the wavelength of entrance ray (0.154 05 nm), B indicates the width of half-height diffraction peak, θ is Bragg angle, the instrumental error and $K_{\alpha 2}$ must be deducted as the calculation is being carried on. Thermal stability measurement of powders was performed on the STA449C differential scanning calorimetry measurement (DSC) made by Crop NETZSCH at a heating rate of 5 ~ 20 ℃/min.

The microstructure observation and analysis of bulk alloys were performed for the bulk alloy on Hitach H-800 TEM with an accelerating voltage of 160 kV. TEM samples were prepared by the method of electrolysis twin-jet and ionization-thinning. The density of bulk alloys after hot-press sintering was measured by Achimedes' law. The measurement of hysterisis loop was performed on the LDJ9600 vibrating sample magnetometer field H_{max} = 955 kA/m.

3 RESULTS AND DISCUSSION

3.1 Preparation of MA powders

Fig. 1 shows the XRD patterns of $Fe_{84}Nb_7B_9$, $Fe_{80}Ti_8B_{12}$ and $Fe_{32}Ni_{36}(Nb/V)_7Si_8B_{17}$ powders after 20 h ball milling. XRD analysis shows that the diffraction peaks of those MA powders in the figure deliver a trendency of peak broadening apparently, and the peak of $Fe_{32}Ni_{36}Nb_7Si_8B_{17}$ owns a characteristic of "steamed bread like". From the analysis of XRD α-Fe supersaturated solid solution forms in $Fe_{84}Nb_7B_9$ and $Fe_{80}Ti_8B_{12}$ alloys; amorphous structure forms in $Fe_{32}Ni_{36}Nb_7Si_8B_{17}$ alloy; γ-(FeNi) supersaturated solid solution and trace content of Fe_2B phase forms in $Fe_{32}Ni_{36}V_7Si_8B_{17}$ alloy. During MA process, a circulatory process of deformation-welded together-break took place in pure elementary powders, which led to serious distortion of lattice, grain refining and a significant increase of the grain boundary's volume fraction. These changes provided driving force and channel for quick-diffusion of solute atoms and made the alloying process perform at atomic level, so solid solution was obtained at last. During the process of solid amorphous transition, thermal chemical diffusibility was always restrained, alltropic phase reaction condition could be obtained, and the melting behavior of solid solution can be considered as a presumptive term of metastable field[22]. Formation of solid amorphous phases was analyzed by thermodynamics, and analysis shows that during MA process, the driving force of solid amorphous formation increases with the increase of supersaturated concentration of solute atoms in α solid solution. When the component of solute atoms approaches the critical value, supersaturation ratio approaches the maximum, and the nucleation of amorphous phase forms. Large concentration fluctuation is prerequisite of amorphous

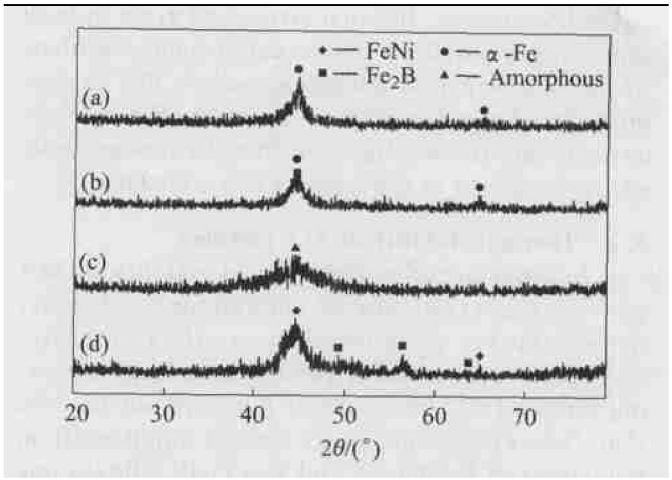

Fig. 1 X-ray diffraction patterns of Fe-based powders after MA for 20 h
(a) —$Fe_{84}Nb_7B_9$; (b) —$Fe_{80}Ti_8B_{12}$; (c) —$Fe_{32}Ni_{36}Nb_7Si_8B_{17}$; (d) —$Fe_{32}Ni_{36}V_7Si_8B_{17}$

phase formation. Refined grains and high microarea lattice distortion provide the formation kinetic condition of amorphous phase. Internal stress and grain growth increasing induced by plastic deformation contribute to the broadening of diffraction peaks. The average grain size of samples can be estimated by Scherrer's equation, and the results show that the average grain size of samples is in the range of 8.0 – 15.0 nm.

3.2 Thermal stability of MA powders

In order to reveal the thermal stability of MA powder(nanocrystalline or amorphous) and select the suitable hot-press temperature, the DSC analysis is performed on these powder samples at a heating rate of 10 ℃/min. From Fig. 2 it can be seen that, two exothermal peaks appear significantly in the curves of $Fe_{84}Nb_7B_9$ and $Fe_{80}Ti_8B_{12}$ alloys, one is the low and flat exothermal peak with wide temperature range (peak value is 374 – 420 ℃), the other is apparent high temperature exothermal peak (peak value is 774 – 710 ℃). The emergence of the first broadening low and flat peak is a common feature of MA powder, which relates to the large distribution range of grain size. The structural relaxation of lattice distorts α-Fe nanocrystalline supersaturated solid solution and the process of nanocrystalline growth[18]. The second exothermal peak is induced by the transformation of α-Fe supersaturated solid solution to α-Fe solid solution intermetallics (Fe_3B and Fe_2B)[8, 18]. From Fig. 2 it can be known that the thermal stability of nanocrystalline microstructure of $Fe_{80}Ti_8B_{12}$ is higher than that of $Fe_{84}Nb_7B_9$, but the decomposition temperature of α-Fe supersaturated solid solution in $Fe_{80}Ti_8B_{12}$ nanocrystalline microstructure is lower than that in $Fe_{84}Nb_7B_9$. Three exothermic peaks appear in the DSC curve of $Fe_{32}Ni_{36}Nb_7Si_8B_{17}$ amorphous powder. The emergence of first low and flat peak is related to the structural relaxation; the second exothermal peak (peak value is 530 ℃) is related to the crystallization of amorphous during the heating up process, in which probably eutectic crystallization reaction takes place, but the manner of crystallization needs to be confirmed. The third exothermic peak (peak value is 760 ℃) may be related to the crystalline transformation of amorphous in remained amorphous with high thermal stability. As $Fe_{32}Ni_{36}V_7Si_8B_{17}$ amorphous powder is concerned, except two exothermic peaks appear as $Fe_{84}Nb_7B_9$ and $Fe_{80}Ti_8B_{12}$, between which a weak exothermic peak (peak value is 431 ℃) appears, and the emergence of this peak is also related to the crystallization transformation of amorphous, which reveals that except α-Fe phase and Fe_2B, there are amorphous phases in $Fe_{32}Ni_{36}V_7Si_8B_{17}$ powder. And the situations of flat exothermic peak and high exothermic peak have a tendency of moving far away. Because of the trace content, the amorphous phase can not be observed by XRD. The thermal stability of these powders depends on the phase component of MA powder.

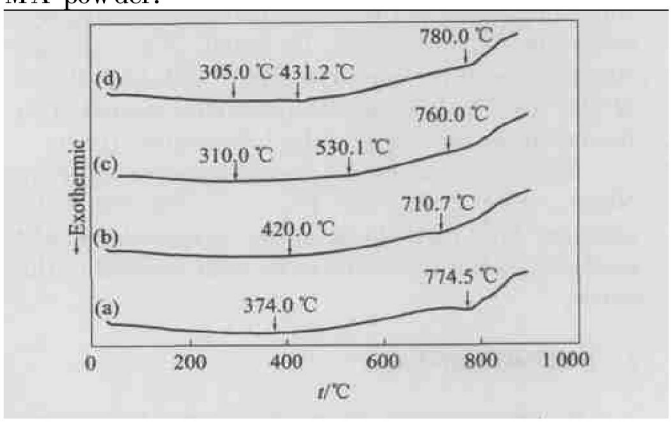

Fig. 2 DSC curves of Fe-based powders after MA for 20 h
(a) —$Fe_{84}Nb_7B_9$; (b) —$Fe_{80}Ti_8B_{12}$;
(c) —$Fe_{32}Ni_{36}Nb_7Si_8B_{17}$; (d) —$Fe_{32}Ni_{36}V_7Si_8B_{17}$

3.3 Preparation of bulk alloys

In order to obtain the bulk alloys with high relative density, with the consideration of DSC analysis finally hot-press temperature is selected as 900 ℃.

Measurement of density shows that, the relative density of $Fe_{84}Nb_7B_9$, $Fe_{80}Ti_8B_{12}$ and $Fe_{32}Ni_{36}$-(Nb/V)$_7Si_8B_{17}$ bulk alloys are 96.7% , 95.5%, 96.8% and 97.4%, respectively.

The XRD patterns of the $Fe_{84}Nb_7B_9$ and $Fe_{80}Ti_8B_{12}$ and $Fe_{32}Ni_{36}$(Nb/V)$_7Si_8B_{17}$ bulk alloys are shown in Fig. 3. Analysis shows that except in $Fe_{80}Ti_8B_{12}$ alloys single phase α-Fe forms; in the other alloys multiphase microstructure forms; $Fe_{84}Nb_7B_9$ alloy is composed of single phase α-Fe and trace content of Fe_2B phase and Fe_3B phase; main nanocrystalline γ-(FeNi) supersaturated solid solution phase and trace content of Fe_2B phase form in $Fe_{32}Ni_{36}$(Nb/V)$_7Si_8B_{17}$ alloy. TEM images of $Fe_{84}Nb_7B_9$, $Fe_{80}Ti_8B_{12}$ and $Fe_{32}Ni_{36}Nb_7Si_8B_{17}$ bulk alloys are shown in Fig. 4. From the TEM images

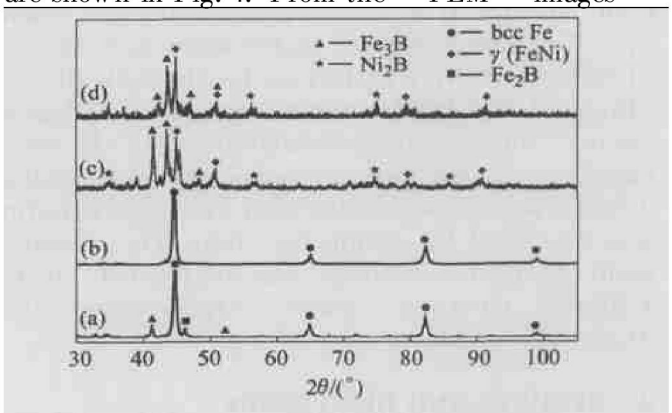

Fig. 3 XRD patterns of hot-press sintering samples
(a) —$Fe_{84}Nb_7B_9$; (b) —$Fe_{80}Ti_7B_{12}$;
(c) —$Fe_{32}Ni_{36}Nb_7Si_8B_{17}$; (d) —$Fe_{32}Ni_{36}V_7Si_8B_{17}$

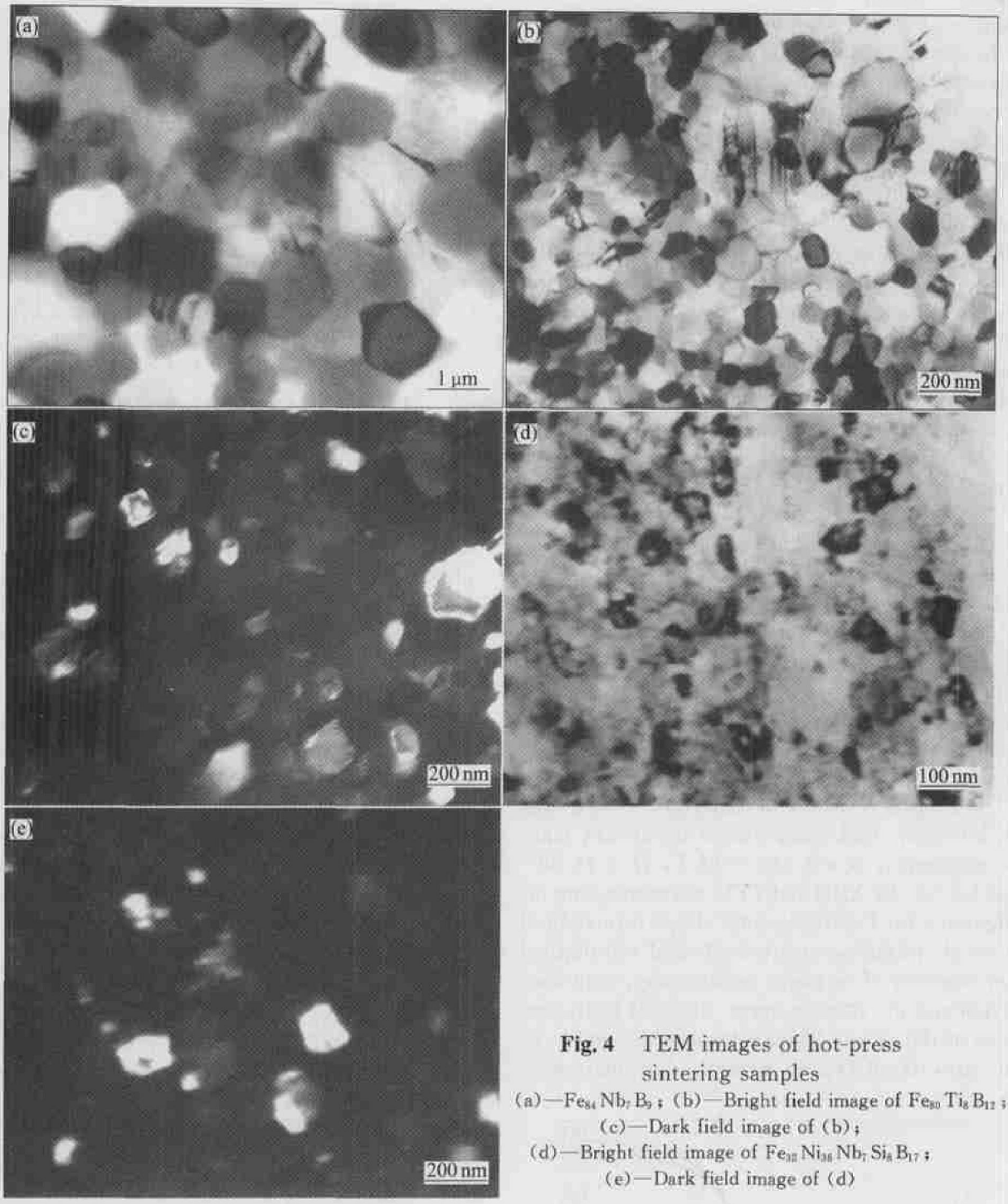

Fig. 4 TEM images of hot-press sintering samples
(a)—$Fe_{84}Nb_7B_9$; (b)—Bright field image of $Fe_{80}Ti_8B_{12}$; (c)—Dark field image of (b); (d)—Bright field image of $Fe_{32}Ni_{36}Nb_7Si_8B_{17}$; (e)—Dark field image of (d)

it can be seen that, the difference in grain size of these bulk alloys is significant. $Fe_{84}Nb_7B_9$ gets a relatively large grain size of 0.3 – 0.8 μm; superfine grains (grain size 50 – 200 nm) are obtained in $Fe_{80}Ti_8B_{12}$ alloy; nanocrystalline microstructure (grain size 20 – 80 nm) are obtained in $Fe_{32}Ni_{36}Nb_7Si_8B_{17}$ alloy.

According to the quantitative relationship between heating rate and the maximum peak temperature of DSC curve proposed by Kissinger et al[23], the apparent activation energy E_p of decomposition of α-Fe phase supersaturated solid solution in $Fe_{84}Nb_7B_9$ and $Fe_{80}Ti_8B_{12}$ MA powders are estimated, and the results show that, the apparent activation energy E_p of $Fe_{84}Nb_7B_9$ is 320.7 kJ/mol, E_p of $Fe_{80}Ti_8B_{12}$ is 447.6 kJ/mol. It can be concluded that: the thermal stability of α-Fe phase supersaturate solid solution in $Fe_{80}Ti_8B_{12}$ alloy is higher than that in $Fe_{84}Nb_7B_9$ alloy. During the process of hot-press sintering, all the as-prepared powders remain nanocrystalline single phase microstructure, however, for the thermal stability of α-Fe phase supersaturated solid solution in $Fe_{80}Ti_8B_{12}$ alloy is higher than that in $Fe_{84}Nb_7B_9$ alloy, and multi-phase microstructure with large grain size forms in $Fe_{84}Nb_7B_9$ bulk alloy, while single phase superfine microstructure formed in $Fe_{80}Ti_8B_{12}$ bulk alloy. By means of TEM observation, it is identified that no second nanophase exists in $Fe_{84}Nb_7B_9$ bulk al-

loy. For $Fe_{32}Ni_{36}Nb_7Si_8B_{17}$ amorphous powder, because of the formation of large quantity of dispersed second phase particles during the process of crystallization transformation of amorphous, multiphase nanocrystalline microstructure forms. Because he multiple phase transformation (eutectoid-crystallization reaction) took place during the process of sintering, these precipitated phases and co-diffussion effect of other atoms restrained the grain boundary growth of γ-(FeNi) phase, so the nanocrystalline grains formed. By means of decreasing the temperature of hot-press sintering and the effect of second-phase dispersed nanoparticles formed in the process of crystallization transformation of amorphous, the nanocrystalline bulk alloys could be obtained by nanocrystalline or amorphous powders.

3.4 Magneic properties of bulk alloys

Hysterisis loop of $Fe_{84}Nb_7B_9$, $Fe_{80}Ti_8B_{12}$ and $Fe_{32}Ni_{36}(Nb/V)_7Si_8B_{17}$ bulk alloys are shown in Fig. 5. Fig. 6 shows the magnetic properties of bulk alloys calculated from the hysterisis loops. As the figures show, the specific saturation magnetization of $Fe_{80}Ti_8B_{12}$ is B_s= 1.74 T, the coercive force H_c= 4.35 kA/m; for $Fe_{84}Nb_7B_9$, B_s= 1.56 T, the coercive force H_c= 8.37 kA/m; Compared to $Fe_{84}Nb_7B_9$ and $Fe_{80}Ti_8B_{12}$, $Fe_{32}Ni_{36}$-$(Nb/V)_7Si_8B_{17}$ bulk alloy owned lower soft magnetic properties, B_s= 0.68 – 0.85 T, H_c= 14.36 – 17.23 kA/m. By XRD and TEM microstructure investigation, for $Fe_{80}Ti_8B_{12}$ bulk alloy, formation of α-Fe single phase supersaturated solid solution led to the decrease of magnetic anisotrophy, magnetostriction and the coercive force. Because of the existence of the second-phase intermetallics and large grain size, H_c of $Fe_{84}Nb_7B_9$ bulk alloy increased. The coercive force of $Fe_{32}Ni_{36}(Nb/V)_7Si_8B_{17}$ bulk alloy increased significantly, which was due to the formation of duplex phase nanocrystalline microstructure composed of γ-(FeNi) phase and the second-phase (Fe_3B, Fe_2B, $Fe_{23}B_6$, Ni_2B). In addition, incomplete densification after hot-press sintering led to the existence of reverse domain boundary of raw powders and the hindrance of magnetic domain wall induced by holes, at the same time, because of internal microstrain induced in hot-press sintering process and the oxidation of powders, coercive force H_c of bulk alloys were increased. It is necessary to study the influence of heat-treatment on magnetic properties.

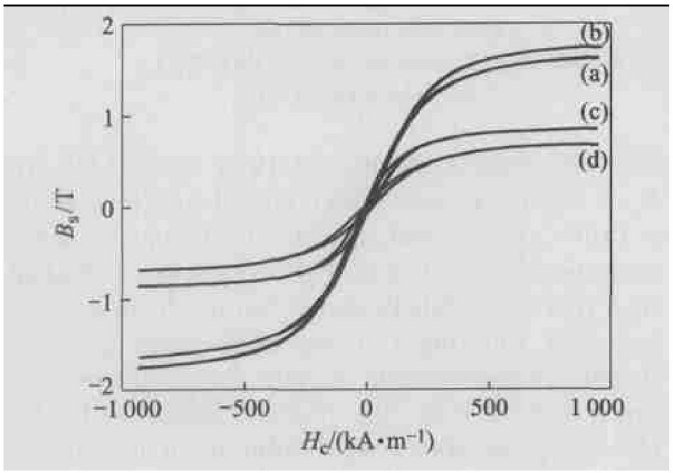

Fig. 5 Hysteresis loops of hot-press sintering samples
(a) —$Fe_{84}Nb_7B_9$; (b) —$Fe_{80}Ti_8B_{12}$; (c) —$Fe_{32}Ni_{36}Nb_7Si_8B_{17}$; (d) —$Fe_{32}Ni_{36}V_7Si_8B_{17}$

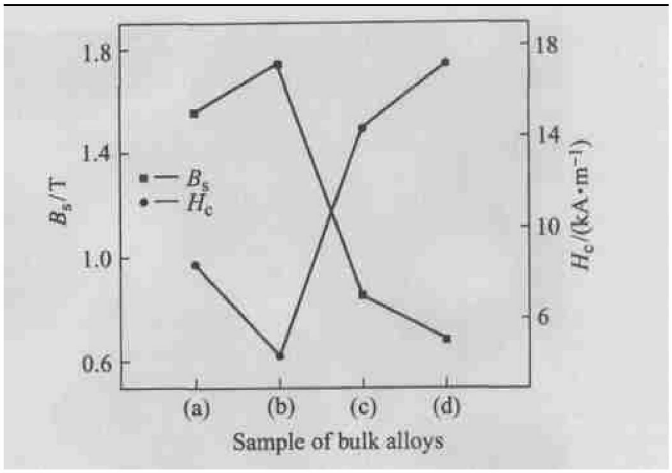

Fig. 6 Magnetic property of hot-press sintering samples
(a) —$Fe_{84}Nb_7B_9$; (b) —$Fe_{80}Ti_8B_{12}$; (c) —$Fe_{32}Ni_{36}Nb_7Si_8B_{17}$; (d) —$Fe_{32}Ni_{36}V_7Si_8B_{17}$

4 CONCLUSIONS

1) After MA for 20 h, α-Fe nanocrystalline single phase supersaturated solid solution forms in $Fe_{84}Nb_7B_9$ and $Fe_{80}Ti_8B_{12}$ alloys; amorphous structure forms in $Fe_{32}Ni_{36}Nb_7Si_8B_{17}$ alloy; duplex microstructure which is composed of nanocrystalline γ-(FeNi) supersaturated solid solution and trace content of Fe_2B phase forms in $Fe_{32}Ni_{36}V_7Si_8B_{17}$ alloy.

2) The decomposition process of supersaturated solid solution phases in $Fe_{84}Nb_7B_9$ and $Fe_{80}Ti_8B_{12}$ alloys happens at 710 – 780 ℃; crystallization reaction in $Fe_{32}Ni_{36}Nb_7Si_8B_{17}$ alloy happens at 530 ℃ (the temperature of peak value) and residual amorphous crystallized further happens at 760 ℃ (the temperature of peak value); phase decomposition process of supersaturated solid solution at 780 ℃ (the temperature of peak value) and crystallization reaction at 431 ℃ (the temperature of peak value) happens in $Fe_{32}Ni_{36}V_7Si_8B_{17}$ alloy.

3) Under 900 ℃, 30 MPa, 0.5 h hot-press sintering conditions, bulk alloys with high relative density (94.7% – 95.8%) can be obtained. Except that the grain size of $Fe_{84}Nb_7B_9$ bulk alloy is large, su-

perfine grains (grain size 50 – 200 nm) are obtained in other alloys. Except that single phase microstructure is obtained in $Fe_{80}Ti_8B_{12}$ bulk alloy, multi-phase microstructures are obtained in other alloys.

4) The magnetic properties of $Fe_{80}Ti_8B_{12}$ bulk alloy (B_s= 1.74 T, H_c= 4.35 kA/m) are significantly superior to those of other bulk alloys, $Fe_{84}Nb_7B_9$ take the second place. $Fe_{32}Ni_{36}(Nb/V)_7Si_8B_{17}$ bulk alloy performs a lower soft magnetic properties, which is related to the different phases of nanocrystalline or amorphous powder forming during hot-press sintering process and grain size.

REFERENCES

[1] Yoshizawa Y, Oguma S, Yamauchi K. New Fe-based soft magnetic alloys composed of ultrafine grain structure [J]. J Appl Phys, 1988, 64: 6044 – 6046.

[2] Suzuki N, Kataoka A, Makino A, et al. High saturation magnetization and soft magnetic properties of bcc Fe-Zr-B alloys with ultrafine grain structure[J]. Mater Trans JIM, 1990, 31(8): 743 – 747.

[3] Suzuki K, Kataoka N, Inoue A, et al. Changes in microstructure and soft magnetic properties of an $Fe_{86}Zr_7B_6Cu_1$ amorphous alloy upon crystallization[J]. Mater Trans JIM, 1991, 32(10): 961 – 968.

[4] Makino A. Nanocrystalline soft magnetic Fe-M-B(M= Zr, Hf, Nb) alloys produced by crystallization of amorphous phase materials transaction[J]. Mater Trans JIM, 1995, 36(7): 924 – 938.

[5] Kawamura Y, Takagi M, Senoo M, et al. Preparation of bulk amorphous alloys by high temperature sintering under a high pressure[J]. Mater Sci Eng, 1988, 98: 415 – 418.

[6] Kawamura Y, Takagi M, Akai M. A newly developed warm extrusion technique for compacting amorphous alloy powders[J]. Mater Sci Eng, 1988, 98: 449 – 452.

[7] Kawamura Y, Inoue A, Kojima A, et al. Consolidation of amorphous Fe-Zr-B powders by hot-pressing method [J]. Journal of the Japan Society of Powder and Powder Metallurgy, 1995, 42(1): 40 – 46.

[8] Kojima A, Horikiri H, Kawamura Y, et al. Production of nanocrystalline b. c. c. Fe-Nb-B bulk alloys by warm extrusion and their magnetic properties[J]. Mater Sci Eng, 1994, A179/A180: 511 – 515.

[9] Kojima A, Horikiri H, Makino A, et al. Soft-magnetic porerties of nanocrystalline bcc Fe-(Nb, Zr)-B bulk alloys consolidated by warm extrusion[J]. Mater Trans JIM, 1995, 36(7): 945 – 951.

[10] Sato T, Taniguchi T, Kondo K, et al. Effect of shock duration time on magnetic properties of dynamically compacted amorphous powder[J]. Journal of the Japan Society of Powder and Powder Metallurgy, 1988, 35 (3): 96 – 100.

[11] QIU Jun, XIE Zi-zhang, YANG Rang, et al. The magnetic properties of the exposive consolidating amorphous powder[J]. Journal of University of Science and Technology Beijing, 1994, 16(4): 330 – 334.

[12] Kawamura Y, Inoue A, Kojima A, et al. Consolidation of amorphous Fe-Zr-B powders by hot-pressing method [J]. Journal of the Japan Society of Powder and Powder Metallurgy, 1995, 42(1): 40 – 46.

[13] Kojima A, Mizushima T, Makino A, et al. Soft magnetic properties of bulk nanocrystalline $Fe_{90}Zr_7B_3$ alloys consolidated by spark-plasma sintering[J]. Journal of the Japan Society of Powder and Powder Metallurgy, 1996, 43(5): 613 – 618.

[14] Shen B L, Kimura H, Inoue A A, et al. Consolidation of Fe-Co-Ga-P-C-B glassy powders by spark-plasma-sintering and their magnetic properties[J]. Journal of the Japan Society of Powder and Powder Metallurgy, 2001, 48(9): 858 – 862.

[15] LI Fan, JI Ya-lin, WU Bing-yao, et al. Fe-Ni-P-B amorphous alloy prepared by mechanical alloying[J]. Acta Metallurgica Sinica, 1999, 35(11): 1183 – 1186.

[16] WANG Jin-hui, ZHU Ru-yang, CHEN Yong-hong, et al. The morphology and microstructure of nanocrystalline $Fe_{1-X}Ni_X$ alloy powders By mechanical alloying [J]. Journal of Functional Materials, 2001, 31(1): 45 – 47.

[17] YANG Jun-you, WU Jian-sheng, ZENG Zhen-peng, et al. Study on mechanical alloying of Fe-M(M= Al, Nb, Si)[J]. Journal of Shanghai Jiaotong University, 1997, 31(9): 142 – 145.

[18] LU Bin, YI Dan-qing, LIU Hui-qun, et al. Preparation of nanocrystalline $Fe_{83}Nb_7B_9Cu_1$ powders by mechanical alloying and their thermal stability[J]. The Chinese Journal of Nonferrous Metals, 2002, 12(6): 1214 – 1217.

[19] Manivel M, Chattopadhyay R K, Majumder B. A narayansamy structure and soft magnetic properties of finemet alloys[J]. Journal of Alloys and Compounds, 2000, 297: 199 – 205.

[20] Huang B, Jiang H G, Perez R J, et al. The effect of Ni on the cryogenic attritor milling of metglas $Fe_{78}B_{13}Si_9$ [J]. Nanostrctured Materials, 1999, 11(8): 1009 – 1016.

[21] Chiriac H, Moga A E, Urse M, et al. Formation and magnetic properties of mechanically alloyed Fe-Cu-Nb-Zr-B nanocrystalline powders[J]. Journal of Magnetism and Magnetic Materials, 1999, 203: 159 – 161.

[22] Fecht H J. Thermodynamic properties of amorphous solids glass formation and glass transition[J]. Materials Transactions JIM, 1995, 36(7): 777 – 793.

[23] LU Wei-chang, XI Tong-geng. Thermoanalysis Mass Spectrometric Method[M]. Shanghai: Shanghai Scientific and Technical Literature Press, 2002.

(Edited by PENG Chao-qun)